ACS Biomaterials SCIENCE & ENGINEERING

pubs.acs.org/journal/abseba

Article

Rapid Detection of SARS-CoV-2 Antigens and Antibodies Using OFET Biosensors Based on a Soft and Stretchable Semiconducting Polymer

Kristina Ditte,[#] Trang Anh Nguyen Le,[#] Oliver Ditzer, Diana Isabel Sandoval Bojorquez, Soosang Chae, Michael Bachmann, Larysa Baraban,* and Franziska Lissel*

Cite This: https://doi.org/10.1021/acsbiomaterials.1c00727

Read Online

ACCESS | Metrics & More | Article Recommendations | Supporting Information

ABSTRACT: In the midst of the COVID-19 pandemic, adaptive solutions are needed to allow us to make fast decisions and take effective sanitation measures, e.g., the fast screening of large groups (employees, passengers, pupils, etc.). Although being reliable, most of the existing SARS-CoV-2 detection methods cannot be integrated into garments to be used on demand. Here, we report an organic field-effect transistor (OFET)-based biosensing device detecting of both SARS-CoV-2 antigens and anti-SARS-CoV-2 antibodies in less than 20 min. The biosensor was produced by functionalizing an intrinsically stretchable and semiconducting triblock copolymer (TBC) film either with the anti-S1 protein antibodies (S1 Abs) or receptor-binding domain (RBD) of the S1 protein, targeting CoV-2-specific RBDs and anti-S1 Abs, respectively. The obtained sensing platform is easy to realize due to the straightforward fabrication of the TBC film and the utilization of the reliable physical adsorption technique for the molecular immobilization. The device demonstrates a high sensitivity of about 19%/dec and a limit of detection (LOD) of 0.36 fg/mL for anti-SARS-Cov-2 antibodies and, at the same time, a sensitivity of 32%/dec and a LOD of 76.61 pg/mL for the virus antigen detection. The TBC used as active layer is soft, has a low modulus of 24 MPa, and can be stretched up to 90% with no crack formation of the film. The TBC is compatible with roll-to-roll printing, potentially enabling the fabrication of low-cost wearable or on-skin diagnostic platforms aiming at point-of-care concepts.

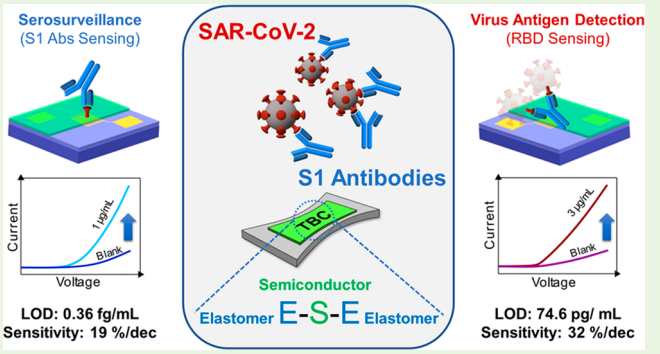

KEYWORDS: *organic field-effect transistors, biosensors, block copolymers, semiconducting polymers, SARS-CoV-2 antigen sensor, anti-SARS-CoV-2 antibodies sensor*

1. INTRODUCTION

The field of bioelectronics develops rapidly, offering novel materials and devices for healthcare applications, e.g., smart biosensors or implants.[1−4] Organic field-effect transistors (OFETs) are prominent members of the biosensors family, due to their good biocompatibility, potential flexibility, and biodegradability, ultimately leading toward wearable and on-skin applications.[5−7] Furthermore, the utilization of solution-processable polymer conjugated semiconductors (PSCs) for the fabrication of OFETs could allow for large-scale and low-cost fabrication, as well as the realization of multiplexed sensing applications.[8,9] A typical OFET device consists of three main components: the terminals (source, drain, and gate electrodes), a dielectric, and an active layer, with the latter formed by an organic semiconductor. Such three-terminal OFET-type devices enable the straightforward amplification and fine-tuning of measured electrical signals by controlling the applied voltage on the gate electrode.[10] In recent years, OFET-based biosensors progressed significantly for the detection of various biofunctional species, e.g., glucose,[11] uric acid,[12] protein,[13] and DNA.[14] Depending on the working mechanism and the final application, the three-terminal OFET-based biosensors can be further divided into conventional OFETs, electrolyte-gated OFETs (EGOFETs), as well as organic electrochemical transistors (OECTs).[15] To provide real-time and continuous health monitoring as a wearable device, the active OFET layer must be adapted to meet the softness and natural stretchability of the skin, which extends by 30% or more.[16] At the same time, the stretchability (i.e., low elastic modulus) of the active layer would enable the higher compliance of the sensor being integrated into the textile or

Special Issue: Bioinspired Materials for Wearable Diagnostics and Biosensors

Received: May 31, 2021
Accepted: August 17, 2021

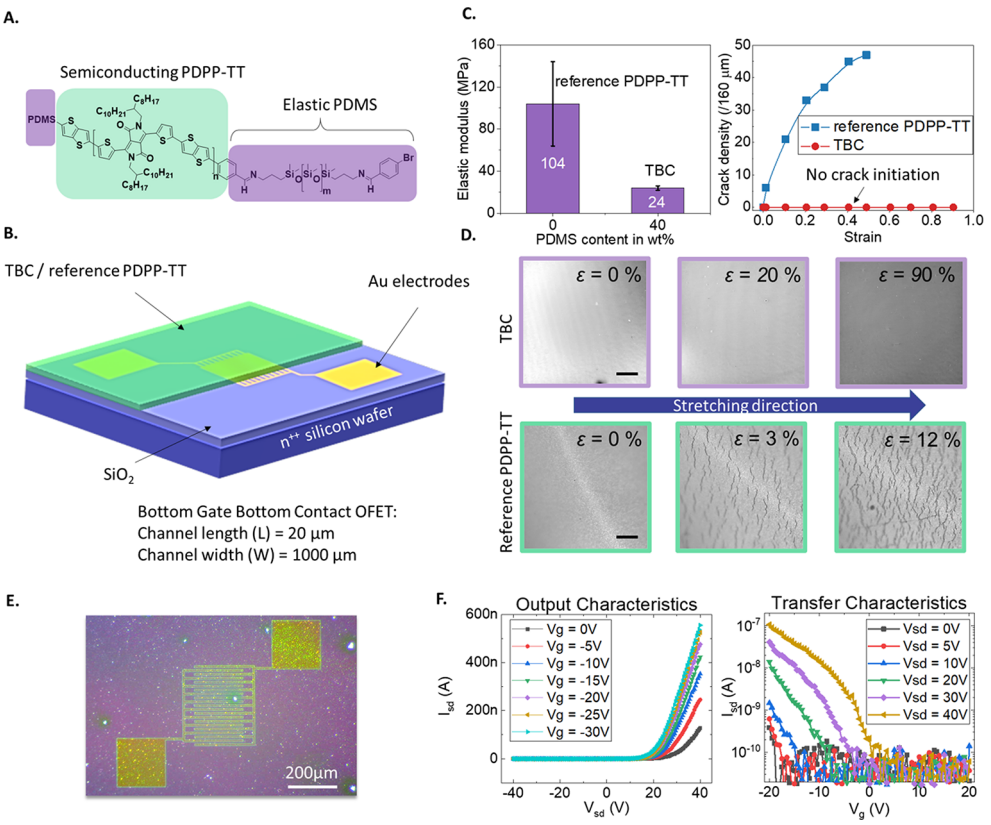

Figure 1. Schematic of the fabricated BGBC OFET and mechanical properties of the analyzed polymers. (A) Chemical structure of the TBC with 40 wt % content of PDMS: light-green highlight denotes semiconducting block PDPP-TT, whereas purple highlight is the elastic PDMS blocks (end-caps). (B) Device configuration using BGBC structure (*Fraunhofer* OFET Gen4, 230 nm SiO_2), where the TBC or reference PDPP-TT polymers were spin-coated on the top of evaporated gold electrodes with L = 20 μm and W = 1000 μm. (C) Left graph: elastic modulus of the reference PDPP-TT copolymer and the TBC with a 40 wt % content of PDMS within the polymer's structure identified by a nanoindentation method (the error bars correspond to the standard deviation due to the softness of the tip). Right graph: crack onset formation of the reference PDPP-TT copolymer and the TBC under stretching. (D) Microscopy images of strained TBC (upper) and reference PDPP-TT (lower), respectively (scale bars denote 20 μm for TBC and 50 μm for the reference PDPP-TT, and ε is the amount of applied strain). (E) Microscopy images of TBC OFETs and (F) electrical characteristics of a typical device.

at the skin, for a more reliable detection of biological signals.[17,18] Another advantage of stretchable biosensors is their noninvasive nature that would lower the barrier in utilizing them in patient's everyday life. Yet, state-of-the-art thin films of PSCs are brittle and prone to mechanical failure upon stretching (already at 1−3% strain).[19] To date, three main methods are available to increase the mechanical compliance of the active material: (i) stress-accommodating engineering (or buckling method),[20] (ii) blending of PSCs into elastomeric matrix or establishing composites,[21] and (iii) molecular engineering.[22,23]

Traditionally, the fabrication of stretchable sensors is driven by strain and pressure sensors, as they are the simplest to realize for on-skin electronic applications, and these sensor types are still of great importance for the realization of continuous health-monitoring devices. By utilizing the buckling method, i.e., laminating the thin organic semiconducting layer on a prestretched elastomer and creating a wrinkled device structure, Kaltenbrunner et al. realized sensors that showed no electrical degradation even at 233% tensile strain.[17] However, this approach requires additional processing steps that increase the final price of a sensor platform, as well as deliver an uneven surface, which limits contact with other device's layers. Wang and co-workers demonstrated a stretchable and self-healable composite of polyaniline, poly(acrylic acid), and phytic acid exhibiting stretchability up to 500% strain, which can be utilized for mechanical sensors to detect a variety of human motions.[24] Despite delivering highly functional hybrid materials, the blending/composite approach requires a precise choice of the blend ratios[25] and, in some cases, specific pretreatment of a semiconducting part.[26]

The utilization of intrinsically soft and semiconducting PSCs could allow for the realization of stretchable OFET biological sensors, yet this approach is challenging: in addition to the problem of the PSC's brittleness, the direct contact of the semiconductor with an aqueous solution is a limiting factor, as it continuously damages the active layer.[27] Consequently, research protocols on such systems are rare. A polyisoindigo-bithiophene-siloxane polymer synthesized by Bao's group is a notable exception: the PSC demonstrated good compatibility with the used microstructured polydimethylsiloxane (PDMS) dielectric layers due to the presence of short siloxane side chains. Almost no hysteresis was detected while measuring the transfer curves of the flexible pressure sensor.[28] Later the same polymer structure was demonstrated to overcome water instability (including seawater), which is preserved over an extended time period.[29] Recently we reported the synthesis of a triblock copolymer (TBC) consisting of a conjugated polydiketo-pyrrolopyrrole-thienothiophene (PDPP-TT) PSC flanked by two soft elastic segments, i.e., PDMS (Figure 1A).[22]

https://doi.org/10.1021/acsbiomaterials.1c00727
ACS Biomater. Sci. Eng. XXXX, XXX, XXX−XXX

PDMS moieties offer not only stretchability but also the possibility to perform reliable physical adsorption of biochemical species, e.g., antibodies or proteins.[30] The utilization of such a block copolymer might therefore serve as a strong foundation to realize a straightforward, low-cost, and wearable biosensing platform.

It has been over a year since the COVID-19 outbreak was declared a pandemic by the World Health Organization (WHO).[31] The high mortality of the SARS-CoV-2 virus (around 3.5 million per year) leads to significant research efforts to develop solutions for a better management of the situation at the societal level. Along with primary means of COVID-19 detection methods, such as polymerase chain reaction (PCR) and paper-based immunosensors, there is a recent interest in exploring other potential virus detection platforms with transistor-based biosensors using advanced materials as a preparation for any future outbreak. These new results present significant improvements in sensing sensitivity, marked by an extremely low limit of detection and short detection times. However, to our knowledge, only electrolyte-gated field effect transistors or organic electrochemical transistors (OECTs) were reported for SARS-CoV-2 antibody and antigen detection so far.[32−34] The need for electrolyte liquid gating in these platforms is a major drawback, as it limits the ability of these devices to be potentially integrated into garments to be used on demand (e.g., when attending social events, sports centers, etc.). Yet such point-of-care systems for quick diagnostics could represent an important part of the solution to the current pandemic situation, as they offer a more flexible route to manage the lock-down conditions.

Here, we present—at the proof-of-concept level—an OFET diagnostics biosensor platform for the detection of SARS-CoV-2 antigen and anti-SARS-CoV-2 antibodies (S1 Abs) on the basis of our previously reported soft and stretchable TBC as an active layer. The physical adsorption technique was demonstrated to be straightforward and fast for biomolecule immobilization.[35] Here, we directly adsorbed SARS-CoV-2 spike receptor-binding domain (RBD) receptors, as well as S1 Abs, onto the TBC surface by immersion into the respective solution. The antigen/polymer (or antibody/polymer) layer is then used for the selective binding of targeted S1 Abs (or RBDs), and the biorecognition effect is detected through direct electronic transduction. Although target incubation was performed in solution, all measurements were carried out in dry-state with the intention of moving toward a more realistic wearable platform. The OFET-based biosensor developed in this study is able to detect the respective analyte in a wide range of concentrations (from 0.1 fg/mL to 1 μg/mL) with a mean detection limit (LOD) of 0.36 fg/mL and a sensitivity of 19%/dec for S1 Abs sensing and or a LOD of 74.6 pg/mL and a sensitivity of 32%/dec for RBD sensing. Therefore, the proposed OFET-based biosensor enables the identification of the presence/absence of an infection, as well as the immune status of the person in one platform. The TBC has favorable mechanical and physical properties, e.g., a low elastic modulus (E_s), and shows no crack formation upon stretching (up to 90%). Considering this, the proposed OFET-based biosensor could be potentially transferred onto stretchable substrates using high-throughput coating techniques and allow for the fabrication of low-cost wearable or on-skin diagnostic platforms.

2. EXPERIMENTAL SECTION

2.1. Materials. The polymers (reference PDPP-TT and TBC) were synthesized after previously reported protocols.[22] Sensing subjects are SARS-CoV-2 S1 RBD protein (P202-021, Trenzyme GmbH) and target molecules human anti-SARS-CoV-2 S1 monoclonal antibody (CABT-CS031, Creative Diagnostics). For testing of the selectivity of the sensor, anti-hOC43 spike antibody (P36334, CUSABIO) and recombinant human coronavirus OC43 spike protein (DEAGC131, Creative Diagnostics) were used. For the verification of unspecific adsorption, we used anti-human specific secondary fluorescence antibodies rabbit anti-human IgG DyLight 488 (SA5-10110, ThermoFisher Scientific) and nonspecific secondary fluorescence goat anti-mouse IgG Alexa Fluor Plus 488 (A32723, ThermoFisher Scientific). Phosphate-buffered saline (PBS) solution was prepared from a tablet (P4417, Sigma-Aldrich) according to the manufacturer's instruction to obtain 0.01 M in concentration, pH = 7.4. Bovine serum albumin (A9418, Sigma Alrich) was diluted in PBS solution at a 0.5 wt % concentration and used without any further purification as a blocking solution.

2.2. Field-Effect Transistor Preparation. Polymer solutions in chlorobenzene at 80 °C, namely, TBC (27 mg mL^{-1}) and reference PDPP-TT (27 mg mL^{-1}), were spin-coated at 1300 and 900 rpm, respectively, on prefabricated bottom-gate bottom-contact field-effect transistor substrates (*Fraunhofer* OFET Gen4, 230 nm SiO_2). The devices were measured afterward with no additional thermal treatment step.

2.3. Surface Functionalization. The surface modification procedure is described in Figure 2B,C. The devices were rinsed with DI water and ethanol and dried with a compressed air gun. In antibody testing strategy: we first immersed the device in 1.5 mL of 3 μg/mL SARS-CoV-2 Spike RBD protein (RBD) in PBS overnight at 4 °C for adsorption. Next, the devices were intensively washed three times using PBS with 0.1% TWEEN 20 surfactant to remove any unbound protein molecules. Bovine serum albumin (BSA) at 0.5 wt % concentration in PBS was used as a blocking solution. The devices were again washed three times with PBS-TWEEN solution. For sensing and detection, we incubated the device in varied concentrations of human anti-SARS-CoV-2 S1 monoclonal antibody (S1 Abs) diluted in PBS for 20 min at room temperature. In the antigen testing strategy, the devices were first immersed in 1.5 mL of 3 μg/mL S1 Abs in PBS overnight at 4 °C. After that, the devices went through a similar procedure of washing and BSA blocking as described in the antibody testing strategy. The detection condition of RBD protein was the same, 20 min at room temperature. For studies of selectivity of the sensor, we incubated the device in 1 μg/mL anti-HuOC43 spike antibody or HuOC43 protein diluted in PBS depending on the sensing strategy (refer to Figure 2B,C). A full calibration curve was constructed for each single device by incubating in increasing analyte concentration (from 0.1 fg/mL to 1 μg/mL) in a stepwise manner. After each incubation, the devices were rinsed with PBS-TWEEN 20 and DI water and dried before measurement.

2.4. Characterization. For the investigation of crack initiation strain, the polymer films were transferred on a PDMS substrate, which was cured at 80 °C for 1 h with a 10:1 mixing ratio of curing agent to base polymer (Sylgard 184, Dow corning), and optical microscopy (MarSurf CM expert, Nanofocus) was performed to obtain the crack images of the polymer film. To apply uniform uniaxial strain on the sample, a custom-made 1D motorized stretching equipment was mounted under the microscope to conduct the measurement. The crack density of the polymer films was evaluated by counting the number of cracks along the cross-section profile in three different lines. Please note that there is a technical limitation to apply a strain of more than 90% on the film; therefore, this value is reported as the final one (Figure 1B).

Optical characterization was performed on an inverted fluorescence microscope with a GFP filter set (Zeiss). Fluorescence secondary antibodies as described in the Materials section were used for the labeling of S1 Abs on the devices. The exposure time was set at 2 s. All

https://doi.org/10.1021/acsbiomaterials.1c00727
ACS Biomater. Sci. Eng. XXXX, XXX, XXX−XXX

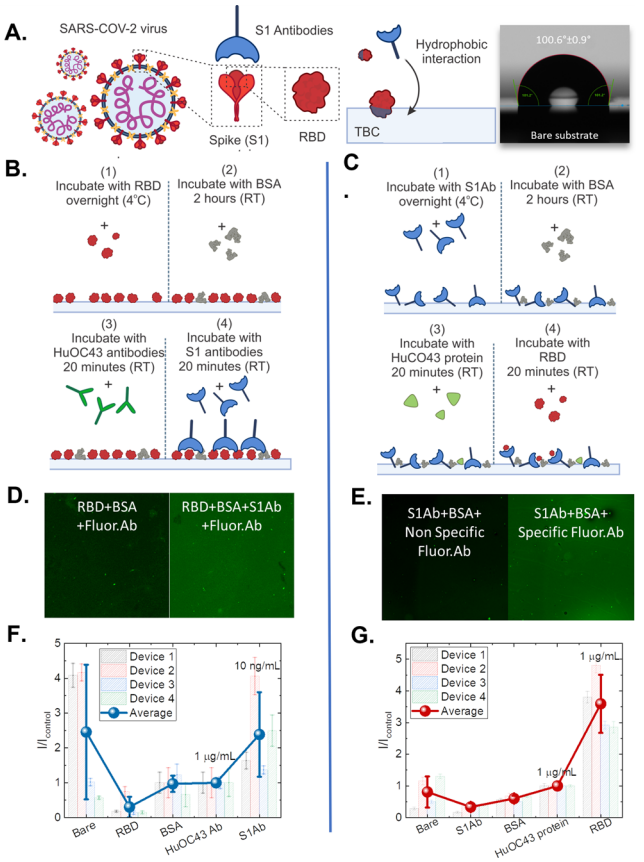

Figure 2. Surface modification of TBC for antigen or antibody sensing. (A) Studied subjects in this work and suggested mechanism for the physisorption of biomolecules to TBC (right picture: contact angle measurement between DI water and TBC). Surface modification procedure for (B) S1 antibody sensing and (C) spike receptor-binding domain (RBD) sensing. (D and E) Fluorescence microscopy images that confirm the success of surface modification. Fluorescence secondary antibodies that have good affinity to S1 Abs (specific fluor. Ab) or no affinity to S1 Abs (nonspecific fluor. Abs) were added to the samples as noted in the images to check the S1 Abs presence on the surface and nonspecific adsorption effect. (F and G) Verification by electrical characterization in two sensing strategies. Output currents at V_g = −20 V and V_{sd} = 40 V were extracted. Bar charts present the current ratio measured at every modification stage to the control (HuOC43 antibody or protein) step collected from 4 OFETs for each sensing strategy. Error bars present the standard deviation of five measurements. Scatter plots show the average and standard error current ratio value of the 4 OFETs.

images were processed by open-source ImageJ software and adjusted for visualization with the same parameters.[36]

Electrical characterization was performed with a Precision Source-meter unit (Keysight, B2902A). Output characteristics were obtained from I−V_{sd} sweeps between −40 and 40 V at V_g = −20 V from OFET with L = 20 μm and W = 1000 μm.

3. RESULTS AND DISCUSSION

3.1. Materials and Crack-Onset Formation. To provide continuous health monitoring via wearable OFET devices on the stretchable substrate, the PSCs must be adapted toward the elasticity of the skin. Recently we reported an intrinsically stretchable and semiconducting TBC based on semiconducting PDPP-TT block covalently end-capped with two elastic PDMS blocks (Figure 1A). The resulting structure possesses around 40 wt % of the insulating elastic moiety. Due to the thermodynamic incompatibility of the two blocks (semiconducting, elastomeric), a phase segregation on the nanoscale occurs, while the inherent properties of each moiety are preserved in the respective phase.[22]

The introduction of elastic PDMS blocks within the PDPP-TT semiconducting backbone resulted in a low elastic modulus (E_s) of the obtained TBC of 24 MPa (compared to the reference copolymer with E_s of 104 MPa)[22] (Figure 1C). To access the mechanical compliance of TBC and the reference polymers, the thin films were transferred on the cross-linked PDMS substrate and stretched with a home-built stretching device up to 90% strain. The morphology of the films was then analyzed with optical microscopy. No crack formation was observed for the TBC block copolymer up to 90% strain, while the reference copolymer started to form cracks already at 1% strain (Figure 1C,D and Figure S1). For the OFET-based biosensor, the TBC and reference PDPP-TT polymers (see the Supporting Information) were spin-coated on bottom gate bottom contact prefabricated OFETs with a channel length (L) of 20 μm and a channel width (W) of 1000 μm, which resulted in a smooth and homogeneous polymer coverage on the device (Figure 1B,E). For a detailed OFET fabrication procedure, please refer to the Experimental Section. A back-gate voltage (V_{bg}) was applied to the silicon substrate (Figure 1B). By sweeping V_{sd} and keeping V_{bg} at a constant value, the output characteristics, I_{sd} (V_{sd}), were obtained, which show a clear p-channel OFET behavior (Figure 1F, left). The transfer curves I_{sd} (V_g) are shown in Figure 1F, right; again, p-type OFET behavior with an ON/OFF ratio of ∼10^4 was observed for V_{sd} = 40 V. As expected, similar OFET characteristics were obtained for the reference PDPP-TT-based device (see Figure S2). The hysteresis and leakage current of transfer curves for the TBC- and PDPP-based OFETs can be found in the Supporting Information (Figures S3−S6).

Moreover, we demonstrated recently that the TBC can be shear-coated at high shearing speeds with almost no change in the electrical performance.[37] These results combined pave the way for this material to be utilized on flexible/stretchable substrates (e.g., foil, cross-linked PDMS) using low-cost and high-throughput coating techniques (e.g., doctor blade, roll to roll printing).

3.2. Surface Functionalization and Fluorescence Measurements. Along with high mechanical compliance of the OFET active layer, the choice of biomaterials' immobilization technique is important to realize a low-cost and high-throughput sensor platform. Physical adsorption is considered a straightforward, inexpensive, and fast technique. Here, the biomaterial is adsorbed on the active material's surface by hydrophobic, ionic, or van der Waals interactions. This method is similar to well-established ELISA protocols that rely mainly on the adsorption of the protein receptors on plastic well plates.[38] In contrast to the covalent surface functionalization, physical adsorption affects the PSCs' properties less and does not need sophisticated chemical designs of the active layer.[39] There are quite a few reports to date based on the physical adsorption of biomolecules on polymer semiconductors. Magliulo et al. realized the adsorption of C-reactive protein (CRP) monoclonal Abs on the poly-3-hexylthiophene (P3HT) layer for the detection of CRP. The electrical performance of the obtained biosensor was comparable to the pristine P3HT OFET, having a detection limit of 2 pM (whereas most immunosensors show a value in the range 0.1−20 mg/L).[40] Likewise, Seshadri et al. utilized physical adsorption of

https://doi.org/10.1021/acsbiomaterials.1c00727
ACS Biomater. Sci. Eng. XXXX, XXX, XXX−XXX

procalcitonin (OCT) specific Abs on the P3HT surface, resulting in a biosensor that could selectively detect OCT at low-picomolar concentrations.[41] However, it is known in the literature that P3HT possesses lower charge carrier mobilities,[8] as well as the fact that it is not stable on ambient conditions,[42] compared to other PSCs, such as polyisoindigo or poly-diketopyrrolopyrrole.

The physical adsorption of biomolecules can then be applied in our OFET platform for the detection of SARS-CoV-2 antigen and antibodies. Unlike PCR, which requires trained staff and expensive equipment, the most current rapid COVID-19 tests are antigen tests that can detect the SARS-CoV-2 virus within half an hour. Meanwhile, when vaccination programs spread around the globe, antibody testing can help determine if the patient produces immunity from the virus. Here, at the proof-of-concept level, we demonstrate the sensing in both directions.

SARS-CoV-2 consists of four major proteins, including spike (S), envelope (E), matrix (M), and nucleocapsid (N). Among them, the S protein suits best for the virus detection platform because of its importance in initiating virus infection.[43] The S protein consists of two subunits: S1 and S2. The S1 protein is responsible for host receptor binding while the S2 protein mediates membrane fusion.[32,44] For antigen testing strategy (Figure 2C), we selected the receptor-binding-domain (RBD) of S1 protein (Figure 2A), which directly interacts with the host receptor as a fingerprint for SARS-CoV-2 virus detection[45] and human anti-SARS-CoV-2 S1 monoclonal antibody (S1 Abs) as a receptor on the sensing surface. For antibody testing (Figure 2B), we immobilized RBD protein on the sensing surface and detected S1 Abs (Figure 2B). The RBD employed in this work contains 223 amino acids with a high percentage of hydrophobic content (see the Supporting Information), which thus fits well for physisorption as the TBC surface is also hydrophobic (contact angle around 100°, Figure 2A). More details about the functionalization step can be found in the Experimental Section.

To confirm the physical adsorption of either RBD or S1 Abs on the active layer surface and its specific adsorption, nonspecific and specific fluorescence secondary antibodies were added to the functionalized surface (Figure 2D,E). Before any addition of fluorescent antibodies, we observed a certain degree of autofluorescence in TCB samples (Figure S7). However, adding nonspecific fluorescent antibodies did not increase the signal in both strategies (Figure 2D,E, left and Figures S7 and S8). This is evidence that there was minimal nonspecific adsorption to the sensing surface after the BSA blocking step. When we added S1 Abs (Figure 2D, right) or specific fluorescent antibodies (Figure 2E, right) to the sample, we observed an increase in the fluorescence signal according to the amount of S1 Abs (Figure S8), which confirms the presence of S1 Abs on the surface. A comparison of the TBC and other polymers, e.g., PDMS, as well as reference polymer PDPP-TT is presented in the Supporting Information (Figures S7 and S8).

To verify each step of the functionalization process, we monitored the electrical characterization of the OFET after each step of the procedure. The source−drain current (I_{sd}) of the OFET device was extracted at V_{sd} = 40 V and V_g = −20 V and normalized to the current level of the control sample (Figure 2F,G), which represent the change after each functionalization step. For each testing strategy, we collected data from four TBC-based OFET devices (bar charts Figure 2F,G). All of them show consistent behavior where they showed a current drop after receptor immobilization, especially after RBD binding, a slight increase in current after BSA blocking step, and a strong escalation after target-molecule binding. Similar behavior was also observed in sensing with PDPP-TT-based OFET devices (Figure S9). Moreover, to test the selectivity of our sensing platform, the modified OFETs were incubated in a high-concentration solution of human coronavirus OC43 antibodies/protein (1 μg/mL) that associated with another type of coronavirus that causes the common flu.[46] The result demonstrates that the I_{sd} remains almost unchanged after this control experiment, which in turn confirms the success of the immobilization method, as well as the selectivity of the RBD/S1 Abs receptors toward binding to S1 Abs/RBD, respectively. Overall, the proposed OFET-based biosensor has great potential for the detection of both antibodies/antigens within one platform.

3.3. Electrical Characterization. The sensing performance was analyzed for OFETs based on TBC within a wide concentration range of S1 Abs and RBD, from 0.1 fg/mL to 1 μg/mL (Figure 3C,D).

As can be seen from Figure 3C, there is a significant escalation of the I_{sd} increase even at very low solution concentrations of S1 Abs. In the case of RBD sensing, the increase in I_{sd} is rather steady from 0.1 fg/mL to 100 pg/mL concentration. Full electrical characterization of a typical TBC-OFET for S1 Abs sensing can be found in Figure S10.

To quantify how the binding of S1 Abs or RBD amplifies the current signal, the ratio between the I_{sd} of each S1 Abs/RBD solution concentration to the I_{sd} of the blank sample (at V_g = −20 V, V_{sd} = 40 V) was calculated (Figure 3E,F). The obtained data for S1 Abs sensing shows that, even at lower S1 Abs solution concentrations, the TBC-based OFET shows a almost three times higher electrical response than the blank PBS response (Figure 3E), indicating extreme sensitivity. The ratio increases almost linearly (R^2 > 0.9) with the S1 Abs concentration. To verify that these results do not originate from the current drifting effect, which might arise from filling interface or bulk trap states of the active layer,[47] the electric measurements of analyzed OFET devices were performed every 20 min for the duration of 140 min (20 min are equal to the incubation time for S1 Abs detection) (Figure S11). The obtained results show that the current ratio caused by the drifting effect is lower and is clearly distinguished compared to the S1 Abs TBC-based OFET sensing signal (Figure 3E,F, gray area). Moreover, the amplification of the current due to the binding of the selectivity control sample is low and lies within the blank noise level, illustrating good selectivity of the sensor. Regarding RBD detection, the sensing response is low at a low concentration of the targeted solution (up to 100 fg/mL), which lies both within the blank error and under the selectivity control detection current level, leading to a higher LOD. This might be explained by the fact that the higher molecular weight of S1Abs results in a nonhomogeneous functionalization and randomly oriented binding centers, which hinder the RBD sensing response (Figure 3B).

On the basis of the obtained electrical data, the LOD and sensitivity were calculated for S1 Abs and RBD sensing over four TBC-based OFET devices (Figure 3G,H). Given the fact that RBD functionalization is more homogeneous (Figure 3A), the mean sensitivity for S1 Abs sensing was calculated to be 19%/dec (best performing device: −24%/dec) over a wide dynamic range, from 0.1 fg/mL to 1 μg/mL, with a confident

https://doi.org/10.1021/acsbiomaterials.1c00727
ACS Biomater. Sci. Eng. XXXX, XXX, XXX−XXX

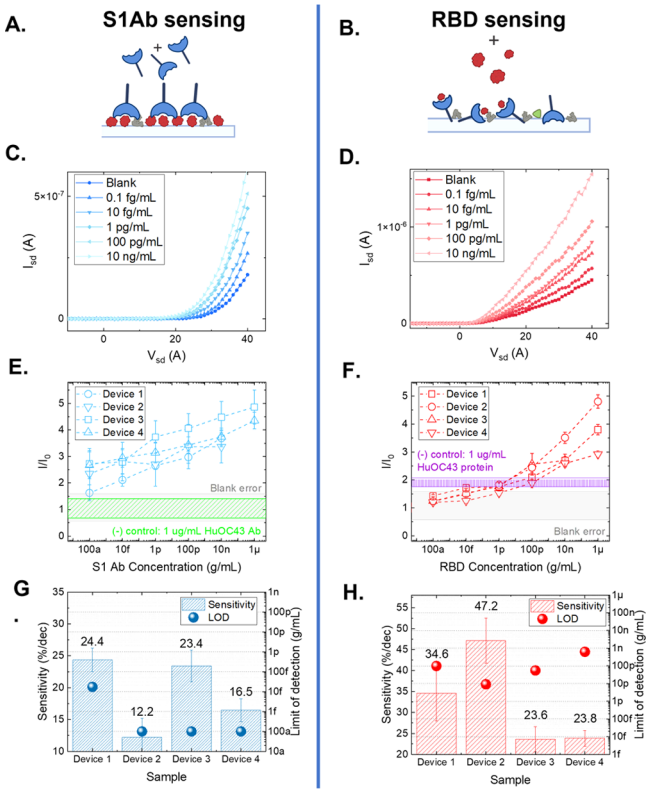

Figure 3. Sensing performance of different detection modes for OFET-based biosensor. (A and B) Schematic representation of the targeted biomaterial (S1 Abs or RBDs) depending on the TBC's surface functionalization. (C and D) Examples of S1 Abs or RBD concentration dependence of output characteristics in TBC-based OFET device. (E and F) Comparison of current ratio to blank sample in the two detection modes. The gray area represents the noise level as a result of current drifting due to consecutive measurements of a blank sample over 2 h. The green and purple bars represent the current level with error of the control sample. The error bars show the standard deviation of five measurements. (G and H) Graphical representation of the determined sensitivity and limit of detection in both detection modes for four different devices. The error bars show the fitting error.

LOD of 0.36 fg/mL (best performing device: −0.1 fg/mL). Although, RBD sensing results in a narrower dynamic range, from 10 pg/mL to 1 μg/mL, and a higher mean LOD of 74.6 pg/mL (best performing device: −9.15 pg/mL), the sensitivity of this mode is significantly better at a high concentration, 32%/dec (best performing device: −47%/dec). Moreover, the TBC-based OFET sensing platform outperformed PDPP-TT-based OFETs in S1 Abs sensing, which shows a lower sensitivity of 17%/dec and a much higher mean LOD f 3.8 ng/mL.

4. CONCLUSIONS

An OFET-based biosensor targeting the anti-SARS-CoV-2 antigen as well as S1 Abs was realized. The sensing platform is easy to realize and utilizes physical adsorption for the molecular immobilization of either S1 Abs or RBD of the S1 protein. The biosensor reported in this study detects a wide dynamic range of concentrations (from 0.1 fg/mL to 1 μg/mL for S1Ab sensing; from 10 pg/mL to 1 μg/mL for RBD sensing) with a mean detection limit of 0.36 fg/mL and a sensitivity of 19%/dec of concentration for S1 Abs sensing and—at the same time—a LOD of 74.6 pg/mL and a sensitivity of 32%/dec for RBD sensing, respectively. In addition, the test is rapid and the result is given within 20 min. The active layer was formed by a triblock copolymer (TBC) consisting of an inner high-performance polymer semiconductor (PDPP-TT) flanked by two soft and elastomeric PDMS chains. Nanoscale phase segregation results in a mechanically soft (E_s = 24 MPa) active layer that can be stretched up to 90% with no crack formation while fully maintaining the necessary electronic functionality. With proper transfer to a stretchable-flexible substrate, the presented concept offers the possibility to realize stretchable biosensors, which might be incorporated in garments or for lab-on-a-mask systems. Ultimately, new wearable platforms might be accessible for on-the-fly detection of antigens and antibodies to aid reducing—and eventually stopping—the spread of COVID-19 and future pandemics.

■ ASSOCIATED CONTENT

Supporting Information

The Supporting Information is available free of charge at https://pubs.acs.org/doi/10.1021/acsbiomaterials.1c00727.

Figures of microscopy images, transfer and output characteristics, concept illustrations, brightness of fluorescence signal, fluorescence images, S1 Abs concentration dependence, comparison of current ratio to blank sample, obtained sensitivity and LOD, drift current measurements, and RBD sequence (PDF)

■ AUTHOR INFORMATION

Corresponding Authors

Franziska Lissel − *Leibniz Institute of Polymer Research Dresden e.V., Dresden 01069, Germany; Faculty of Chemistry and Food Chemistry, Dresden Technical University, Dresden 01062, Germany; Institute of Organic Chemistry and Macromolecular Chemistry, Friedrich Schiller University Jena, Jena 07743, Germany;* orcid.org/0000-0003-0254-4565; Email: lissel@ipfdd.de

Larysa Baraban − *Institute of Radiopharmaceutical Cancer Research, Helmholtz-Zentrum Dresden-Rossendorf, Dresden 01328, Germany;* orcid.org/0000-0003-1010-2791; Email: l.baraban@hzdr.de

Authors

Kristina Ditte − *Leibniz Institute of Polymer Research Dresden e.V., Dresden 01069, Germany; Faculty of Chemistry and Food Chemistry, Dresden Technical University, Dresden 01062, Germany*

Trang Anh Nguyen Le − *Institute of Radiopharmaceutical Cancer Research, Helmholtz-Zentrum Dresden-Rossendorf, Dresden 01328, Germany; Faculty of Medicine Carl Gustav Carus, Dresden Technical University, Dresden 01307, Germany*

Oliver Ditzer − *Leibniz Institute of Polymer Research Dresden e.V., Dresden 01069, Germany; Faculty of Chemistry and Food Chemistry, Dresden Technical University, Dresden 01062, Germany*

Diana Isabel Sandoval Bojorquez − *Institute of Radiopharmaceutical Cancer Research, Helmholtz-Zentrum Dresden-Rossendorf, Dresden 01328, Germany*

Soosang Chae − *Leibniz Institute of Polymer Research Dresden e.V., Dresden 01069, Germany*

https://doi.org/10.1021/acsbiomaterials.1c00727
ACS Biomater. Sci. Eng. XXXX, XXX, XXX−XXX

Michael Bachmann − *Institute of Radiopharmaceutical Cancer Research, Helmholtz-Zentrum Dresden-Rossendorf, Dresden 01328, Germany; Faculty of Medicine Carl Gustav Carus, Dresden Technical University, Dresden 01307, Germany*

Complete contact information is available at: https://pubs.acs.org/10.1021/acsbiomaterials.1c00727

Author Contributions

#K.D. and T.A.N.L. contributed equally. The manuscript was written through contributions of all authors. All authors have given approval to the final version of the manuscript.

Notes

The authors declare no competing financial interest.

■ ACKNOWLEDGMENTS

This work was financially supported by the Deutsche Forschungsgemeinschaft (DFG, German Research Foundation) under the project ID 436376809. F.L. would like to thank the Fonds der Chemischen Industrie (FCI) for a Liebig Fellowship. L.B. acknowledges the support of the DFG (project number: ID 413655771). L.B. and M.B. would like to thank the SAB for the support in the project Nr. 5044119002. S.C. would like to thank the Alexander von Humboldt foundation for a postdoctoral fellowship.

■ REFERENCES

(1) Frank, J. A.; Antonini, M. J.; Anikeeva, P. Next-Generation Interfaces for Studying Neural Function. *Nat. Biotechnol.* **2019**, *37* (9), 1013−1023.

(2) Someya, T.; Bao, Z.; Malliaras, G. G. The Rise of Plastic Bioelectronics. *Nature* **2016**, *540* (7633), 379−385.

(3) Karnaushenko, D.; Ibarlucea, B.; Lee, S.; Lin, G.; Baraban, L.; Pregl, S.; Melzer, M.; Makarov, D.; Weber, W. M.; Mikolajick, T.; Schmidt, O. G.; Cuniberti, G. Light Weight and Flexible High-Performance Diagnostic Platform. *Adv. Healthcare Mater.* **2015**, *4* (10), 1517−1525.

(4) Jeon, D.-Y.; Pregl, S.; Park, S. J.; Baraban, L.; Cuniberti, G.; Mikolajick, T.; Weber, W. M. Scaling and Graphical Transport-Map Analysis of Ambipolar Schottky-Barrier Thin-Film Transistors Based on a Parallel Array of Si Nanowires. *Nano Lett.* **2015**, *15*, 4578−4584.

(5) Shi, W.; Guo, Y.; Liu, Y. When Flexible Organic Field-Effect Transistors Meet Biomimetics: A Prospective View of the Internet of Things. *Adv. Mater.* **2020**, *32* (15), 1901493.

(6) Wang, J.; Ye, D.; Meng, Q.; Di, C.; Zhu, D. Advances in Organic Transistor-Based Biosensors. *Adv. Mater. Technol.* **2020**, *5* (7), 2000218.

(7) Perinot, A.; Giorgio, M.; Mattoli, V.; Natali, D.; Caironi, M. Organic Electronics Picks Up the Pace: Mask-Less, Solution Processed Organic Transistors Operating at 160 MHz. *Adv. Sci.* **2021**, *8* (4), 2001098.

(8) Yang, J.; Zhao, Z.; Wang, S.; Guo, Y.; Liu, Y. Insight into High-Performance Conjugated Polymers for Organic Field-Effect Transistors. *Chem.* **2018**, *4* (12), 2748−2785.

(9) Blasi, D.; Viola, F.; Modena, F.; Luukkonen, A.; MacChia, E.; Picca, R. A.; Gounani, Z.; Tewari, A.; Österbacka, R.; Caironi, M.; Kovacs Vajna, Z. M.; Scamarcio, G.; Torricelli, F.; Torsi, L. Printed, Cost-Effective and Stable Poly(3-Hexylthiophene) Electrolyte-Gated Field-Effect Transistors. *J. Mater. Chem. C* **2020**, *8* (43), 15312−15321.

(10) Torsi, L.; Magliulo, M.; Manoli, K.; Palazzo, G. Organic Field-Effect Transistor Sensors: A Tutorial Review. *Chem. Soc. Rev.* **2013**, *42* (22), 8612−8628.

(11) Furusawa, H.; Ichimura, Y.; Nagamine, K.; Shiwaku, R.; Matsui, H.; Tokito, S. Detection of 1,5-Anhydroglucitol as a Biomarker for Diabetes Using an Organic Field-Effect Transistor-Based Biosensor. *Technologies* **2018**, *6* (3), 77.

(12) Liao, C.; Mak, C.; Zhang, M.; Chan, H. L. W.; Yan, F. Flexible Organic Electrochemical Transistors for Highly Selective Enzyme Biosensors and Used for Saliva Testing. *Adv. Mater.* **2015**, *27* (4), 676−681.

(13) Macchia, E.; Manoli, K.; Holzer, B.; Di Franco, C.; Ghittorelli, M.; Torricelli, F.; Alberga, D.; Mangiatordi, G. F.; Palazzo, G.; Scamarcio, G.; Torsi, L. Single-Molecule Detection with a Millimetre-Sized Transistor. *Nat. Commun.* **2018**, *9* (1), 3223.

(14) Shi, W.; Yu, X.; Zheng, Y.; Yu, J. DNA Based Chemical Sensor for the Detection of Nitrogen Dioxide Enabled by Organic Field-Effect Transistor. *Sens. Actuators, B* **2016**, *222*, 1003−1011.

(15) Lee, Y. H.; Jang, M.; Lee, M. Y.; Kweon, O. Y.; Oh, J. H. Flexible Field-Effect Transistor-Type Sensors Based on Conjugated Molecules. *Chem.* **2017**, *3* (5), 724−763.

(16) Annaidh, A. N.; Ottenio, M.; Bruyère, K.; Destrade, M.; Gilchrist, M. D. Mechanical Properties of Excised Human Skin. *IFMBE Proc.* **2010**, *31*, 1000−1003.

(17) Kaltenbrunner, M.; Sekitani, T.; Reeder, J.; Yokota, T.; Kuribara, K.; Tokuhara, T.; Graz, I.; Bauer-gogonea, S.; Bauer, S.; Someya, T.; Drack, M.; Schwo, R. An Ultra-Lightweight Design for Imperceptible Plastic Electronics. *Nature* **2013**, *499*, 458−463.

(18) Root, S. E.; Savagatrup, S.; Printz, A. D.; Rodriquez, D.; Lipomi, D. J. Mechanical Properties of Organic Semiconductors for Stretchable, Highly Flexible, and Mechanically Robust Electronics. *Chem. Rev.* **2017**, *117* (9), 6467−6499.

(19) Wang, G. J. N.; Shaw, L.; Xu, J.; Kurosawa, T.; Schroeder, B. C.; Oh, J. Y.; Benight, S. J.; Bao, Z. Inducing Elasticity through Oligo-Siloxane Crosslinks for Intrinsically Stretchable Semiconducting Polymers. *Adv. Funct. Mater.* **2016**, *26* (40), 7254−7262.

(20) Kaltenbrunner, M.; White, M. S.; Głowacki, E. D.; Sekitani, T.; Someya, T.; Sariciftci, N. S.; Bauer, S. Ultrathin and Lightweight Organic Solar Cells with High Flexibility. *Nat. Commun.* **2012**, *3*, 1−7.

(21) Xu, J.; Wang, S.; Wang, G. N.; Zhu, C.; Luo, S.; Jin, L.; Gu, X.; Chen, S.; Feig, V. R.; To, J. W. F.; Rondeau-gagné, S.; Park, J.; Schroeder, B. C.; Lu, C.; Oh, J. Y.; Wang, Y.; Kim, Y.; Yan, H.; Sinclair, R.; Zhou, D.; Xue, G.; Murmann, B.; Linder, C.; Cai, W.; Tok, J. B.; et al. Highly Stretchable Polymer Semiconductor Films through the Nanoconfinement Effect. *Science (Washington, DC, U. S.)* **2017**, *355*, 59−64.

(22) Ditte, K.; Perez, J.; Chae, S.; Hambsch, M.; Al-Hussein, M.; Komber, H.; Formanek, P.; Mannsfeld, S. C. B.; Fery, A.; Kiriy, A.; Lissel, F. Ultrasoft and High-Mobility Block Copolymers for Skin-Compatible Electronics. *Adv. Mater.* **2021**, *33*, 2005416.

(23) Wu, H.-C.; Lissel, F.; Wang, G.-J. N.; Koshy, D. M.; Nikzad, S.; Yang, H.; Xu, J.; Luo, S.; Matsuhisa, N.; Cheng, Y.; et al. Metal−Ligand Based Mechanophores Enhance Both Mechanical Robustness and Electronic Performance of Polymer Semiconductors. *Adv. Funct. Mater.* **2021**, *31* (11), 2009201.

(24) Wang, T.; Zhang, Y.; Liu, Q.; Cheng, W.; Wang, X.; Pan, L.; Xu, B.; Xu, H. A Self-Healable, Highly Stretchable, and Solution Processable Conductive Polymer Composite for Ultrasensitive Strain and Pressure Sensing. *Adv. Funct. Mater.* **2018**, *28* (7), 1705551.

(25) Gumyusenge, A.; Tran, D. T.; Luo, X.; Pitch, G. M.; Zhao, Y.; Jenkins, K. A.; Dunn, T. J.; Ayzner, A. L.; Savoie, B. M.; Mei, J. Semiconducting Polymer Blends That Exhibit Stable Charge Transport at High Temperatures. *Science (Washington, DC, U. S.)* **2018**, *362*, 1131−1134.

(26) Choi, D.; Kim, H.; Persson, N.; Chu, P.; Chang, M.; Kang, J.; Graham, S.; Reichmanis, E. Elastomer − Polymer Semiconductor Blends for High-Performance Stretchable Charge Transport Networks. *Chem. Mater.* **2016**, *28* (4), 1196−1204.

(27) Bobbert, P. A.; Sharma, A.; Mathijssen, S. G. J.; Kemerink, M.; De Leeuw, D. M. Operational Stability of Organic Field-Effect Transistors. *Adv. Mater.* **2012**, *24* (9), 1146−1158.

(28) Schwartz, G.; Tee, B. C. K.; Mei, J.; Appleton, A. L.; Kim, D. H.; Wang, H.; Bao, Z. Flexible Polymer Transistors with High

Pressure Sensitivity for Application in Electronic Skin and Health Monitoring. *Nat. Commun.* **2013**, *4* (May), 1859.
(29) Knopfmacher, O.; Hammock, M. L.; Appleton, A. L.; Schwartz, G.; Mei, J.; Lei, T.; Pei, J.; Bao, Z. Highly Stable Organic Polymer Field-Effect Transistor Sensor for Selective Detection in the Marine Environment. *Nat. Commun.* **2014**, *5*, 1−9.
(30) Khnouf, R.; Karasneh, D. Polydimethyl Siloxane Microfluidic Channel Protein Functionalization Techniques A Study on Methodologies and Optimum Conditions. *IEEE 11th Annu. Int. Conf. Nano/Micro Eng. Mol. Syst.* **2016**, 409−413.
(31) WHO. *Coronavirus Disease 2019 (COVID-19): Situation Report − 52*. https://www.who.int/docs/default-source/coronaviruse/situation-reports/20200312-sitrep-52-covid-19.pdf?sfvrsn=e2bfc9c0_4 (accessed 2021-08-27).
(32) Seo, G.; Lee, G.; Kim, M. J.; Baek, S. H.; Choi, M.; Ku, K. B.; Lee, C. S.; Jun, S.; Park, D.; Kim, H. G.; Kim, S. J.; Lee, J. O.; Kim, B. T.; Park, E. C.; Kim, S. Il. Rapid Detection of COVID-19 Causative Virus (SARS-CoV-2) in Human Nasopharyngeal Swab Specimens Using Field-Effect Transistor-Based Biosensor. *ACS Nano* **2020**, *14* (4), 5135−5142.
(33) Shao, W.; Shurin, M. R.; Wheeler, S. E.; He, X.; Star, A. Rapid Detection of SARS-CoV-2 Antigens Using High-Purity Semiconducting Single-Walled Carbon Nanotube-Based Field-Effect Transistors. *ACS Appl. Mater. Interfaces* **2021**, *13* (8), 10321−10327.
(34) Guo, K.; Wustoni, S.; Koklu, A.; Díaz-Galicia, E.; Moser, M.; Hama, A.; Alqahtani, A. A.; Ahmad, A. N.; Alhamlan, F. S.; Shuaib, M.; Pain, A.; McCulloch, I.; Arold, S. T.; Grünberg, R.; Inal, S. Rapid Single-Molecule Detection of COVID-19 and MERS Antigens via Nanobody-Functionalized Organic Electrochemical Transistors. *Nat. Biomed. Eng.* **2021**, *5*, 666−677.
(35) Fu, Y.; Romay, V.; Liu, Y.; Ibarlucea, B.; Baraban, L.; Khavrus, V.; Oswald, S.; Bachmatiuk, A.; Ibrahim, I.; Rümmeli, M.; Gemming, T.; Bezugly, V.; Cuniberti, G. Chemiresistive Biosensors Based on Carbon Nanotubes for Label-Free Detection of DNA Sequences Derived from Avian Influenza Virus H5N1. *Sens. Actuators, B* **2017**, *249*, 691−699.
(36) Schindelin, J.; Arganda-Carreras, I.; Frise, E.; Kaynig, V.; Longair, M.; Pietzsch, T.; Preibisch, S.; Rueden, C.; Saalfeld, S.; Schmid, B.; Tinevez, J. Y.; White, D. J.; Hartenstein, V.; Eliceiri, K.; Tomancak, P.; Cardona, A. Fiji: An Open-Source Platform for Biological-Image Analysis. *Nat. Methods* **2012**, *9* (7), 676−682.
(37) Ditte, K.; Kiriy, N.; Perez, J.; Hambsch, M.; Mannsfeld, S. C. B.; Krupskaya, Y.; Maragani, R.; Voit, B.; Lissel, F. Charge Carrier Mobility Improvement in Diketopyrrolopyrrole Block-Copolymers by Shear Coating. *Polymers (Basel, Switz.)* **2021**, *13*, 1435.
(38) Lequin, R. M. Enzyme Immunoassay (EIA)/Enzyme-Linked Immunosorbent Assay (ELISA). *Clin. Chem.* **2005**, *51* (12), 2415−2418.
(39) Hammock, M. L.; Knopfmacher, O.; Naab, B. D.; Tok, J. B.; Bao, Z. Investigation of Protein Detection Parameters Using Nanofunctionalized Organic Field-Effect Transistors. *ACS Nano* **2013**, *7* (5), 3970−3980.
(40) Magliulo, M.; De Tullio, D.; Vikholm-Lundin, I.; Albers, W. M.; Munter, T.; Manoli, K.; Palazzo, G.; Torsi, L. Label-Free C-Reactive Protein Electronic Detection with an Electrolyte-Gated Organic Field-Effect Transistor-Based Immunosensor. *Anal. Bioanal. Chem.* **2016**, *408* (15), 3943−3952.
(41) Seshardi, P.; Manoli, K.; Schneiderhan-Marra, N.; Anthes, U.; Wierzchowiec, P.; Bonrad, K.; Franco, C. Di; Torsi, L. Low-Picomolar, Label-Free Procalcitonin Analytical Detection with an Electrolyte-Gated Organic Field-Effect Transistor Based Electronic Immunosensor. *Biosens. Bioelectron.* **2018**, *104*, 113.
(42) Choi, S.; Jeong, J. W.; Jo, G.; Ma, B. C.; Chang, M. Conjugated Polymer/Paraffin Blends for Organic Field-Effect Transistors with High Environmental Stability. *Nanoscale* **2019**, *11* (20), 10004−10016.
(43) Huang, Y.; Yang, C.; Xu, X.-F.; Xu, W.; Liu, S.-W. Structural and Functional Properties of SARS-CoV-2 Spike Protein: Potential Antivirus Drug Development for COVID-19. *Acta Pharmacol. Sin.* **2020**, *41* (9), 1141−1149.
(44) Tai, W.; He, L.; Zhang, X.; Pu, J.; Voronin, D.; Jiang, S.; Zhou, Y.; Du, L. Characterization of the Receptor-Binding Domain (RBD) of 2019 Novel Coronavirus: Implication for Development of RBD Protein as a Viral Attachment Inhibitor and Vaccine. *Cell. Mol. Immunol.* **2020**, *17* (6), 613−620.
(45) Premkumar, L.; Segovia-Chumbez, B.; Jadi, R.; Martinez, D. R.; Raut, R.; Markmann, A.; Cornaby, C.; Bartelt, L.; Weiss, S.; Park, Y.; Edwards, C. E.; Weimer, E.; Scherer, E. M.; Roupael, N.; Edupuganti, S.; Weiskopf, D.; Tse, L. V.; Hou, Y. J.; Margolis, D.; Sette, A.; Collins, M. H.; Schmitz, J.; Baric, R. S.; Silva, A. M. de. The RBD Of The Spike Protein Of SARS-Group Coronaviruses Is A Highly Specific Target Of SARS-CoV-2 Antibodies But Not Other Pathogenic Human and Animal Coronavirus Antibodies. *medRxiv Prepr*, in press, 2020.
(46) Lim, Y.; Ng, Y.; Tam, J.; Liu, D. Human Coronaviruses: A Review of Virus−Host Interactions. *Diseases* **2016**, *4* (4), 26.
(47) Lindner, T.; Paasch, G.; Scheinert, S. Influence of Distributed Trap States on the Characteristics of Top and Bottom Contact Organic Field-Effect Transistors. *J. Mater. Res.* **2004**, *19* (7), 2014−2027.

https://doi.org/10.1021/acsbiomaterials.1c00727
ACS Biomater. Sci. Eng. XXXX, XXX, XXX−XXX